



Evaluation of characteristic parameters for high performance hall cells



Maria-Alexandra Paun^{a,*}, Jean-Michel Sallese^b, Maher Kayal^b

^a High Voltage Microelectronics and Sensors (HVMS) Group, Department of Engineering, University of Cambridge, 9 JJ Thomson Avenue, Cambridge CB3 0FA, United Kingdom

^b STI-IEL-Electronics Laboratory, Ecole Polytechnique Fédérale de Lausanne (EPFL), CH-1015 Lausanne, Switzerland

ARTICLE INFO

Article history:

Received 12 December 2013

Received in revised form

3 February 2014

Accepted 17 April 2014

Available online 17 May 2014

Keywords:

Hall cells

Three-dimensional physical simulations

Hall voltage

Absolute sensitivity

Offset

Temperature effects

Hall mobility

ABSTRACT

The current work focuses on presenting specific Hall cells with high performance, and their corresponding parameters. The design, integration, measurements and model development for their performance assessment are necessary stages considered in the generation of the Hall cells. Experimental results regarding the Hall cells absolute sensitivity, offset and offset temperature drift are provided for two particular structures exhibiting the best behavior in terms of maximum sensitivity and lowest offset. Three-dimensional physical simulations were performed for the structures and the Hall mobility was extracted. Representation of the inverse of the geometrical correction factor for the Greek-cross Hall cell is also provided.

© 2014 Elsevier Ltd. All rights reserved.

1. Introduction

The Hall Effect sensors are used in many applications, for example in the DC brushless motor, for the contactless measurements of mechanical quantities like position or angle. They are also used for direct magnetic field sensing, as in electronic compasses. Silicon Hall sensors are often prime candidates for such applications due to their cost-effective integration potential, reflected in low cost, robustness and versatility [1].

CMOS technology has also the advantage of easy co-integration with electronics on the same chip. The Hall Effect is based on magnetic field influence acting perpendicularly on a semiconducting structure carrying a certain electric current. Due to the fact that the charge carriers moving in a magnetic field are subject to a Lorentz force, a so-called Hall voltage is induced in the device in a direction perpendicular to the current flow. New research is devoted to submicron Hall Effect sensors which are nowadays used for the detection of the supermagnetic beads [2].

As it is known, the principal accuracy limitations that affect Hall Effect sensors performances are the offset and its temperature drift [3]. Potential sources of offset generation are related to the fabrication process of a Hall cell, packaging, operating conditions and ageing [4]. The major source for the offset voltages apparition is the imbalances of the Hall plate. Therefore, a real Hall sensor could have a zero-field

offset due to possible geometrical mismatches. In order to eliminate the offset of Hall sensors, the dynamic method known as “current-spinning technique” is used [5–8]. An important figure of merit of these sensors is the sensitivity which is strongly limited by the short-circuit effects. A high absolute sensitivity improves the signal-to-noise ratio of magnetic sensors [9].

Compact models of cross-shaped Hall sensors have recently been developed [10]. The performance of the horizontal Hall sensors in CMOS technology has been greatly improved over the last years. Hall devices with offset less than 10 μV [11] and integrated Hall sensors with an offset drift lower than 1.5 $\mu\text{T}/^\circ\text{C}$ [12] were reported.

Extensive analysis of the geometry influence on the Hall cells performance was presented in various recent papers by the authors, which also provided three-dimensional simulations for their assessment and proposed a large experimental database for the parameters that govern their behavior, especially the offset [13–17].

The work in this paper aims at presenting two different Hall cells which can be used for high performance achievement. The proposed structures were integrated in a 0.35 μm CMOS technology and thoroughly tested amongst others for sensitivity, offset and offset drift. The objectives were to select Hall cells able to provide a low offset (below 30 μT) at the room temperature and a low offset temperature drift (less than 0.3 $\mu\text{T}/^\circ\text{C}$), a few times lower than the state-of-the-art.

Section 2 is devoted to Hall cells geometrical considerations and Hall cells design parameters. Section 3 incorporates the experimental results obtained for two particular Hall cells, regarding offset voltages, magnetic equivalent residual offset at room

* Corresponding author.

E-mail address: map65@cam.ac.uk (M.-A. Paun).

temperature versus the biasing current and its temperature drift. Section 4 focuses on the results obtained by the three-dimensional simulations used to predict the Hall cells performance. At this point, the Hall mobility is extracted and commented. Finally, the paper concludes with the emphasis on the two proposed Hall cells selected for minimum offset and offset drift and high absolute sensitivity respectively.

2. Hall cells geometrical considerations

2.1. Hall voltage and sensitivity

Any Hall Effect device is characterized by the Hall voltage V_{HALL} , given as follows:

$$V_{HALL} = \frac{Gr_H}{nqt} I_{bias} B \quad (1)$$

where B is the magnetic field induction, G is the geometrical correction factor, I_{bias} is the biasing current, r_H is the Hall scattering factor, n is the carrier density and t is the thickness of the active region [18]. In the case of silicon, the Hall scattering factor is usually 1.15.

The geometrical correction factor, G , models the reduction of V_{HALL} due to the part of the current which flows through the sensing contacts. It is worthwhile mentioning that there are different symmetrical shapes for the Hall cells, such as plate, cross, square and other. The geometrical correction factor G tries to answer to the geometry variance and Hall voltage modification for a cell having a certain shape.

Sensitivity is one of the most important figures of merit related to a sensor. In general, the sensitivity is defined as the change in output resulting from a given change in input. Consequently, both absolute and relative sensitivities can be introduced. All the equations below are introduced exactly as in Popovic's book [18]. Firstly, the absolute sensitivity of a Hall magnetic sensor is considered as given by the equation below:

$$S_A = \left| \frac{V_{HALL}}{B} \right| = \frac{Gr_H}{nqt} I_{bias} \quad (2)$$

The ratio between the absolute sensitivity and a certain bias quantity accounts for bias-related sensitivity. Secondly, the current-related sensitivity S_I has the following relation:

$$S_I = \frac{S_A}{I_{bias}} = \left| \frac{1}{I_{bias}} \frac{V_{HALL}}{B} \right| \text{ and } V_{HALL} = S_I I_{bias} B \quad (3)$$

The units of S_I are $VA^{-1} T^{-1}$.

2.2. Geometrical correction factor

In the literature, the expression of the geometrical correction factor G has been obtained by conformal mapping, for various shapes of Hall cells. The formulae, different for each configuration, are valid under some accuracy limitations and only work for certain relationships between the geometrical parameters (length, width, contacts length, etc.) of the corresponding cell.

In this paper, we were interested to analyze the Greek cross shape. For the classical Greek-cross with contacts on each side, the expression of the geometrical correction factor G [19] is given by the following expression:

$$G = 1 - 7.896 m \cotan(\theta_H) \exp\left(\frac{-\pi}{2\lambda}\right), \lambda \rightarrow 0 \quad (4)$$

The equation above is valid for λ approaching 0, where the parameter λ denotes the ratio of the sum of the lengths of the

contacts c and the length of the boundary b .

$$\lambda = \frac{c}{b} \quad (5)$$

Further on, m is defined through the Hall angle θ_H with the aid of the formula:

$$\theta_H = \frac{m\pi}{2} = \arctan(\mu B) \quad (6)$$

By consequence, m is defined as follows:

$$m = \frac{2\theta_H}{\pi} \quad (7)$$

It is to be mentioned that there are other equivalent formulae for the geometrical correction factor G for the Greek-cross cell which use the relations in the length and width of the cell (L and W , respectively). More details about the Hall cells geometrical parameters can be found in [13,14].

The importance of the geometry in high sensitivity achievement was investigated by the authors in previous papers [13,20]. To this purpose, maximization of the geometrical correction factor for structures with small sensing contacts was performed. A high sensitivity can be achieved in a Greek-cross structure with large contacts and high L/W , but also in a rectangular Hall structure with very small sensing contacts.

For the Greek cross case, the three-dimensional representation of the inverse of the geometrical correction factor G versus m and λ is represented in Fig. 1.

2.3. Hall cells design

A dozen of different Hall cells were integrated in a $0.35 \mu m$ CMOS technology, in two silicon runs. We will focus in this paper on only two of them, XL and square Hall cells respectively.

The XL Hall cell is a scaled version of a basic Greek cross cell. This configuration was chosen in order to minimize the errors of the contour which become less important in this case, due to their averaging on a greater size. This assumption is confirmed experimentally as well. The square cell has very small sensing contacts for high absolute sensitivity achievement, but the location of the contacts on the p-n junction and the small size of this cell could possibly increase the offset.

This section presents the Hall cells specific design considerations and summarizes the geometrical parameters for two of the integrated Hall cells, displaying the highest sensitivity (square) and both the lowest offset and temperature drift (XL) respectively. Detailed offset measurements results are presented in Section 3.

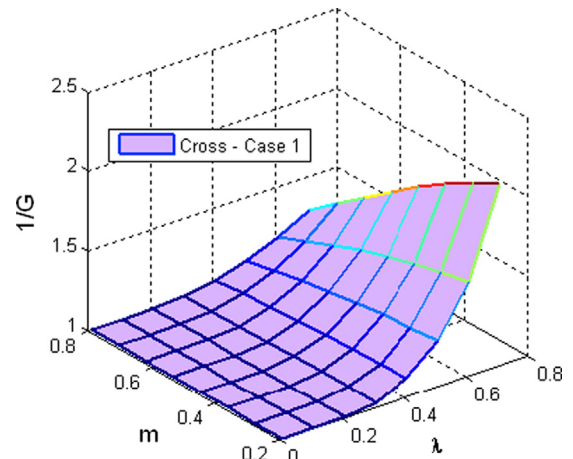


Fig. 1. $1/G$ versus m and λ , for cross Hall structures.

The sensitivity measurements were performed by subjecting the samples to a perpendicular magnetic field of $B=0.497$ T.

The two analyzed geometries, together with their specific parameters are presented in Table 1. W, L stand for the width and length of the active region (n -well) of the Hall devices while s represents the sensing contact length respectively. For the two Hall structures, the geometrical correction figure of merit G was computed using the formulae presented in [18].

3. Experimental results

The performance of the Hall cells is given by the analysis of their absolute sensitivity, the zero-magnetic field offset voltage and their corresponding temperature drifts. Therefore, in achieving Hall cells with good performance, a high sensitivity and a low offset drift are required.

3.1. Hall cells offset and its temperature drift

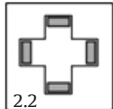
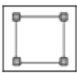
Extensive measurements regarding single and residual offset, as well as the temperature drift were performed by the authors and published in recent papers [13,15].

3.1.1. Experimental results for offset at room temperature

Basically, the offset is a parasitic voltage that adds to the Hall voltage:

$$V_{out} = V_{HALL} + V_{offset} \quad (8)$$

Table 1
Hall cells design parameters.

Hall cell	XL	Square
Geometry (planar representation)		
R_0 (k Ω) @ $T=300$ K, $B=0$ T	2.2	4.9
S_A (V/T) @ $I_{bias}=0.5$ mA	0.0412	0.0467
L (μ m)	43.2	20
W (μ m)	19	20
L/W	2.27	1
Contacts dimensions s (μ m)	18.3	2.3
Geometrical correction factor (G)	0.86	0.96

By making use of the dynamic current-spinning or connection-commutation technique [18], where the biasing current virtually rotates at 90° , the residual offset is significantly decreased as an average on several phases:

$$V_{offset} = \frac{1}{no. of phases} \sum_{i=1}^{no. of phases} V_i \quad (9)$$

where V_i is the individual offset of each phase, expressed in volts. In this context, a phase is considered an interchange in the set of biasing and sensing contacts. For example, the residual offset can be obtained as a result of 2-phase or 4-phase averaging.

According to Popovic's book, in order to characterize the error which appears when measuring the magnetic induction caused by the offset, one would need to compute the magnetic induction which creates a Hall voltage equal to the offset voltage. By consequence, we have the following formula:

$$B_{offset} = \frac{V_{offset}}{S_A} \quad (10)$$

where V_{offset} is the one previously defined and S_A is the absolute sensitivity. This quantity is also called offset-equivalent magnetic field.

To obtain the data in Figs. 2 and 3 (a), the biasing current was ramped, and the four-phase residual offset in V was measured. The experimental data is processed and presented for biasing currents of interest up to 0.7 mA and absolute sensitivity of approximately 0.06V/T.

We were then interested in the variation of the magnetic field equivalent residual offset as a function of the biasing current, for the proposed Hall cells. When computing the magnetic field equivalent residual offset, the curves used for the sensitivity (V/T) for each cell were obtained under a constant magnetic field, generated by a NMR permanent magnet of magnetic induction $B=0.497$ T, perpendicular to the probe.

Figs. 2 and 3 (b) display the magnetic field equivalent residual offset characteristics at room temperature with respect to the absolute sensitivity, for two of the proposed Hall cells, where each geometry is replicated and measured 8 times on the chip, at different positions.

It is to be mentioned that the residual offset is not a direct function of the sensitivity, but an implicit one via the biasing current. However, for more meaningfulness, we decided to display this information versus the absolute sensitivity, as it is useful to know how much residual offset corresponds to a certain sensitivity. The indications in the legend represent the specific positions of

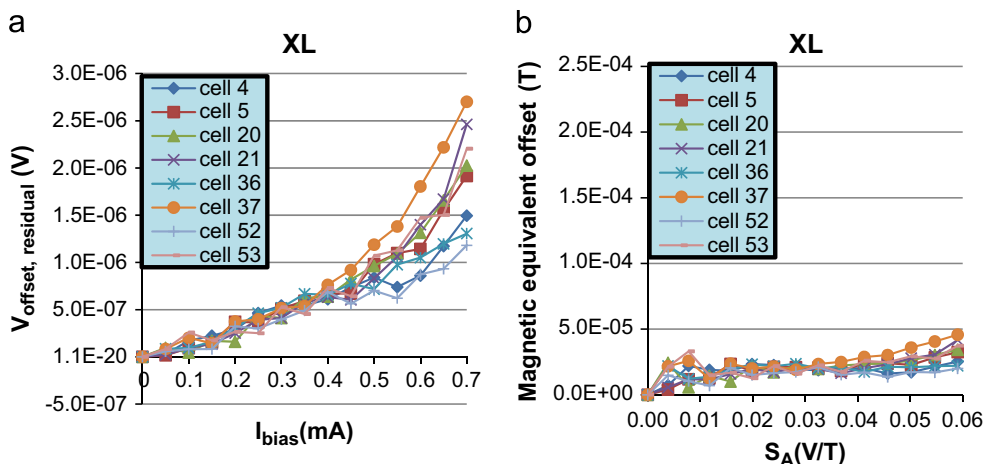


Fig. 2. Measured residual offset (V) vs. I_{bias} (a) and magnetic equivalent offset vs. S_A (b), for the XL Hall cell.

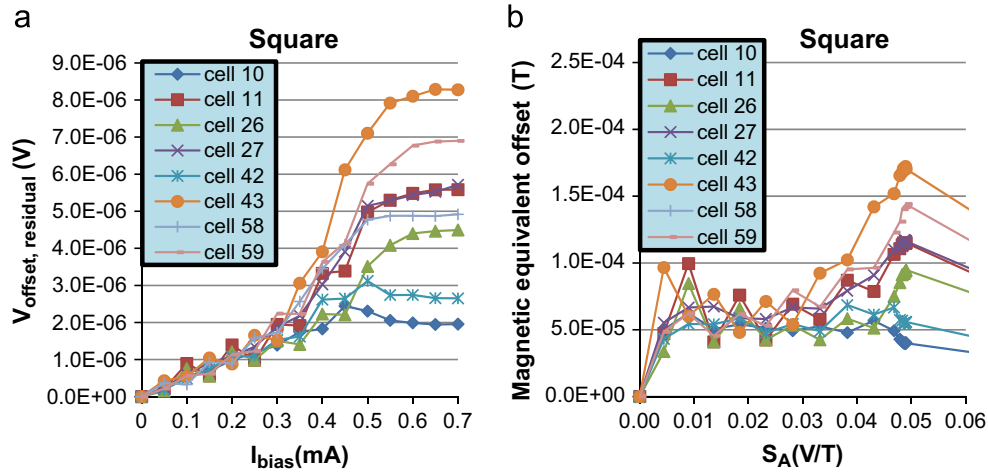


Fig. 3. Measured residual offset (V) vs. I_{bias} (a) and magnetic equivalent offset vs. S_A (b), for the square Hall cell.

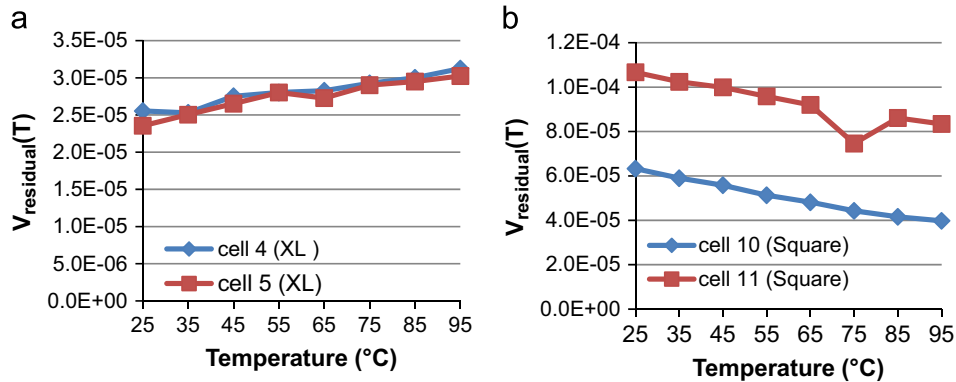


Fig. 4. Measured magnetic equivalent residual offset (T) versus temperature for XL Hall cell (a) and square Hall cell (b).

the cells within a chip containing 64 cells. As the sensitivity at low current values may be disturbed by measurements errors, in Figs. 2 and 3 (b), the reliable measurements are the ones for sensitivities above $0.01V/T$.

We can observe from these graphs, the XL cell displays the lowest magnetic equivalent offset for the range of the sensitivity considered values. We have therefore identified the cell having the best performance in terms of minimum offset at room temperature.

3.1.2. Experimental results for offset drift

The on-chip compensation of the temperature dependent offset drift of a Hall sensor was discussed in various papers [21–24]. The drift in the silicon integrated sensors due to their thermo-mechanical stresses is analyzed in [25–27], while the drift of the magnetic sensitivity due to moisture absorbed by the IC package is presented in [28].

The residual offset temperature variation was measured for the integrated Hall cells. A Temprotonic oven was used to cycle the temperature between $25\text{ }^{\circ}\text{C}$ and $95\text{ }^{\circ}\text{C}$. When analyzing the offset, the same cell was considered and tested twice on the chip. The aim was to see the possible variance of the offset with the position on the chip. Fig. 4 presents the magnetic equivalent residual offset in Tesla plotted against the temperature for two of the integrated Hall cells.

The offset information in the graphs above, for the two Hall cells integrated within the first silicon run, is obtained with the automated measurement setup, earlier on presented [15]. The

advantage of this setup is once again proven, by the immediate and accurate release of the residual offset data. It is to be noted that for the XL cell, the offset temperature drift was computed for a biasing current of $I_{bias} = 1\text{ mA}$. Meanwhile, for the square structure, the biasing current was reduced to $I_{bias} = 0.5\text{ mA}$ to avoid the saturation region, as for this particular Hall cell its measured input resistance is higher than the resistance of the XL device.

4. Results and discussion

4.1. Basic considerations of the three-dimensional physical simulations

In order to get a reliable analysis of the real devices behavior, the simulations in three spatial dimensions should be used, as they give the most accurate results. Therefore, to predict the Hall cells performance, three-dimensional physical simulations were performed.

By using the Synopsys Sentaurus TCAD tool [29], which solves the Poisson equation, both electrons and holes continuity equations, three-dimensional simulations of Hall Effect sensors were performed. A 3D numerical modeling of carrier transport process in the magnetic field (electrostatic potential, current distributions) for semiconductor magnetic sensors with different geometries is used.

At each point of the grid, three unknowns will be considered, namely V , n , p . Further on, we would need three equations and the corresponding boundary conditions to solve the nonlinear system

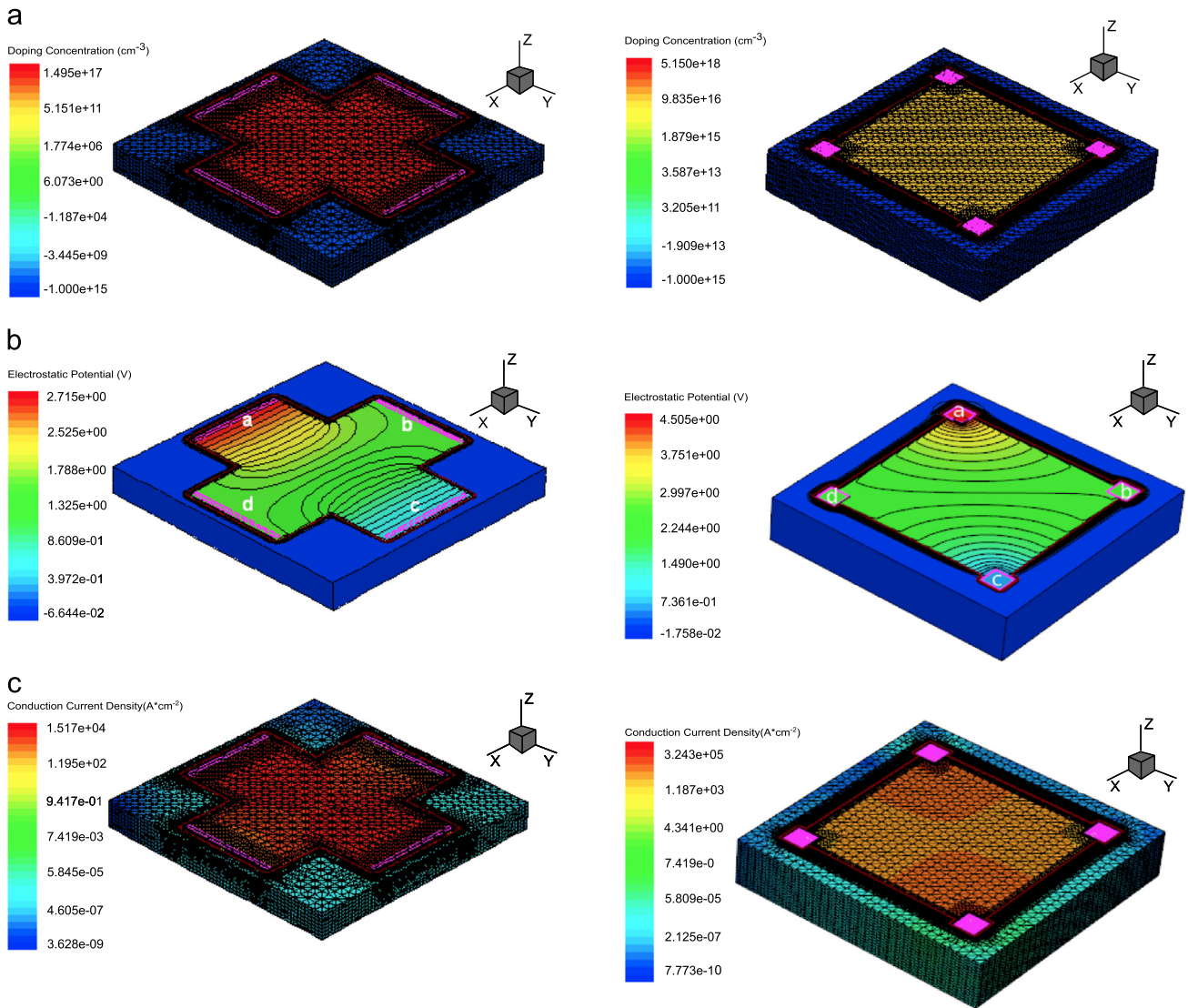


Fig. 5. Three-dimensional representation through meshed structure with doping concentration (a), electrostatic potential distribution (b), conduction current density (c) for XL Hall cell (left hand side) and Square Hall cell (right hand side) respectively.

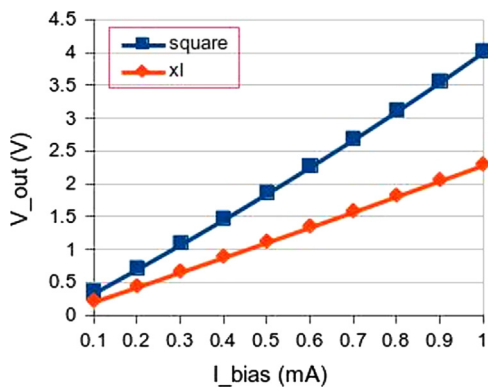


Fig. 6. Simulated I-V characteristics of the Hall cells.

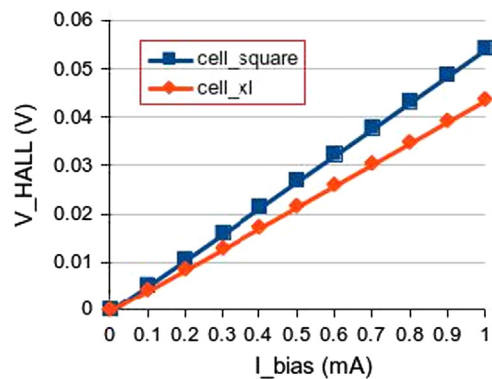


Fig. 7. Simulated V_{HALL} vs. I_{bias} for the Hall cells.

of partial differential equations. In order to have a correct solution, the discretization of the Poisson's equation, electron and holes continuity equations will be needed and a coupled method, which is a generalization of the Newton method, will be used to compute the initial proposed system by numerical iterative procedure.

The magnetic field acting on the semiconductor structure for Hall voltage generation was handled by the galvanic transport model, which is the model used for carrier transport in magnetic fields. More precisely, the more general class of phenomena called galvanomagnetic effects consists amongst other of the Hall Effect and the magnetoresistance effect [18] Galvanomagnetic effects are

the manifestations of charge transport phenomena in condensed matter in the presence of a magnetic field.

By considering the electric field direction as a reference, the Hall Effect could be defined as a transverse isothermal galvanomagnetic effect. On the other hand, the magnetoresistance effect is considered as a longitudinal isothermal galvanomagnetic effect. Galvanomagnetic effects also include different galvanothermoelectric effects. A theoretical understanding of galvanomagnetic effects could be explored in more depth in different books, [30,31].

Mobility was considered via doping dependence formula and recombination processes were taken into account via Shockley–Read–Hall and Auger model as considered in paper [32]. In this context, the ohmic contacts are assumed ideal and the contact regions support a sufficiently high dopant concentration. In the used simulator, the carrier concentrations at the ohmic contact region are given by charge neutrality and equilibrium conditions while the electrostatic potential is prescribed by the classical Dirichlet type conditions [29].

The analysis of magnetic field effects in semiconductor devices is done by solving the transport equation of electrons and holes inside the device. The usual drift-diffusion model of the carrier densities \vec{J}_n and \vec{J}_p should be rewritten by taking into account the magnetic field-dependent terms issued by the effect of Lorentz force on the carriers. Sentaurus includes the effect of magnetic field on semiconductors within the galvanic transport model.

4.2. Hall cells three-dimensional models

For example, amongst the Hall cells which were previously integrated and tested, we will consider two of them, for strict performance specifications achievement. On one hand, the XL Hall cell has the lowest offset and offset temperature drift. On the other hand, the square Hall cell has a higher absolute sensitivity. For this purpose, we decided to thoroughly investigate these two particular sensors by three-dimensional physical simulations.

In the next figures, the three-dimensional models of the XL and Square Hall cells are depicted. The XL cell was developed and also presented in previous papers [13,16,17]. Detailed simulations for other various Hall cells are incorporated in other recent papers of the authors [13] and in the PhD thesis of the first author [33]. Circuit models for Hall cells including temperature effects were developed by the authors in recent paper [34,35]. The Square cell is for the first time emphasized in details and modeled in the present work.

In Fig. 5, the meshed silicon Hall structures are shown, namely the doping concentration distribution (a), the electrostatic potential distribution (b), as well as the conduction current density isolines c), for the XL Hall cell on the left-hand side and Square Hall cell on the right-hand side, respectively. The 3D Hall cells mesh contained a sufficient number of points for a good tradeoff between accuracy and simulation run time. Small meshing dimensions and a high number of points increase the accuracy of the results, but take more CPU time and longer to execute.

It is to be mentioned that the simulated Hall structures are equipped with four electrodes (depicted in pink), which were named with letters from *a* to *d*. This notation is not to be confused with the variables used in Eq. (5).

In general these sensors are highly symmetric structures and invariant to an orthogonal rotation. Because any geometrical mismatch could significantly increase the offset, all the cells were accurately modeled. The present analysis is focused on the XL and Square Hall cells. The implemented structures were intended to have the same fabrication process which is close to the one used when integrating the real Hall sensors. The Hall cells were all modeled on a Silicon p-substrate with an n-well active region.

The exact XFAB CMOS fabrication process parameters are not provided by the foundry. By consequence, we proceeded to using

parameter extraction from measurements and numerical computations such that the simulated structures to follow as closely as possible the previously integrated and tested Hall devices. Therefore, a p-substrate with a Boron concentration of 10^{+15} cm^{-3} and an active n-well region doped with Arsenic of peak concentration $1.5 \cdot 10^{+17} \text{ cm}^{-3}$, in the form of a Gaussian profile implantation were used. This doping profile allows an average mobility of $0.0630 \text{ m}^2 \text{ V}^{-1} \text{ s}^{-1}$ at the surface of the devices. The thickness is $5 \mu\text{m}$ for the p-substrate and $1 \mu\text{m}$ for the implantation of the n-doped profile active region respectively.

For the case of the Square cell, as the contacts are situated on the p-n junctions, additional n+ regions were used for the contacts with a concentration $n_+ = 10^{+19} \text{ cm}^{-3}$, therefore the color coded legend is different for the Square cell in Fig. 5(a), on the right-hand side. The magnetic field is considered at the value $B=0.5 \text{ T}$.

The current–voltage characteristics of the two simulated Hall cells, as well as the simulated Hall voltage versus the biasing current are displayed in Figs. 6 and 7, respectively. It is to be noted that the simulated input resistance was computed as the slope of the curves from Fig. 6. It accounts for $R_{in}=4.07 \text{ k}\Omega$ for the Square cell and $R_{in}=2.31 \text{ k}\Omega$ for the XL cell. At a biasing current of 1 mA , the Hall voltage is approximately 54 mV for the Square cell and 43 mV for the XL cell. This is an increase of approximately 25%, which is primarily explained by the increase of the geometrical correction factor *G*.

4.3. Hall mobility evaluation

The Hall mobility is an important parameter to investigate in the study of Hall cells performance. The data in the following figures has been extracted using the simulator and is shown for both considered Hall cells.

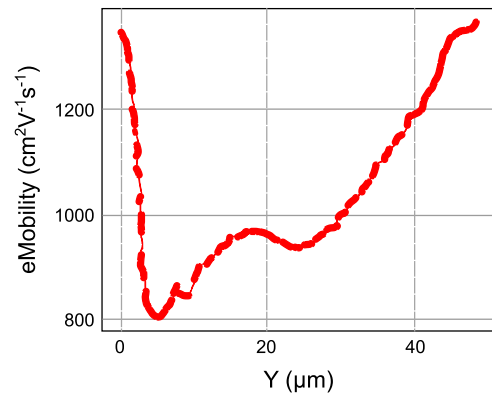


Fig. 8. The electron mobility versus Oy axis for XL cell.

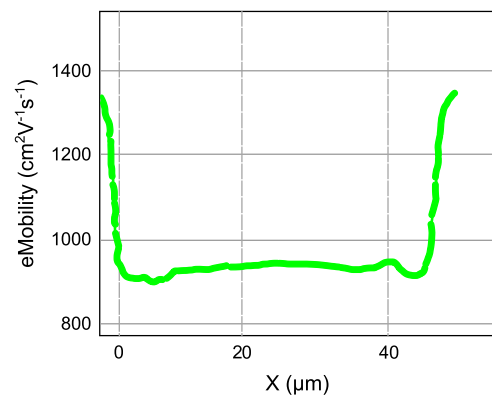


Fig. 9. The electron mobility versus Ox axis for XL cell.

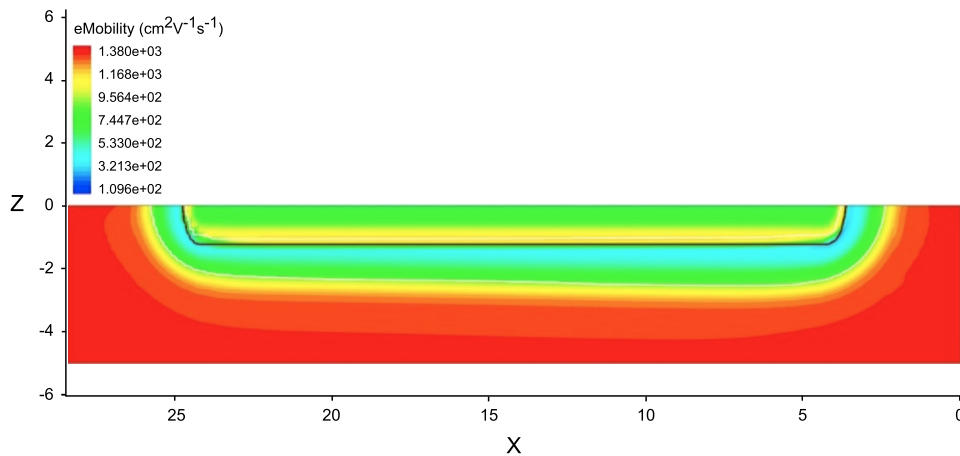


Fig. 10. The electron mobility color coded distribution for Square cell.

The electron mobility (in this case the Hall mobility) is presented in Figs. 8 and 9 above, as extracted on the three-dimensional simulated XL structure with cuts on Ox ($X=19.92 \mu\text{m}$) and Oy ($Y=23.115 \mu\text{m}$) respectively.

We can observe in Fig. 8 a minimum value for the electron mobility ($\mu_H=800 \text{ cm}^2 \text{ V}^{-1} \text{ s}^{-1}$), obtained around $Y=4.5 \mu\text{m}$, then an increase to around $\mu_H=970 \text{ cm}^2 \text{ V}^{-1} \text{ s}^{-1}$.

In Fig. 9, we can notice a plateau for the Hall mobility $\mu_H=950 \text{ cm}^2 \text{ V}^{-1} \text{ s}^{-1}$ for x -coordinate in the interval $10\text{--}40 \mu\text{m}$. In Fig. 10, whose axes are in μm units, the Hall electron mobility of the square Hall cell is provided. It has been obtained by cutting the initial 3D Square drawing at $Z=0 \mu\text{m}$, then for an additional cut at $Y=14.2 \mu\text{m}$.

5. Conclusions

In the present paper the characteristic parameters of Hall cells with high performance have been investigated. The aim of the work was to propose Hall cells geometries which will guarantee good behavior.

For the Greek-cross Hall cell, the three-dimensional representation of the inverse of the geometrical correction factor G was analyzed. Experimental results obtained with an automated measurement setup were provided for the offset voltages, magnetic equivalent residual offset, residual offset temperature drift, etc.

Among the integrated and tested Hall cells, two particular structures proved to exhibit the highest performance. The XL cell proved to be a good candidate for minimal offset and offset temperature drift, while the square structure provided the maximum sensitivity. To predict the performance of various Hall cells prior to design and integration, three-dimensional physical simulations were performed. The information on Hall mobility was extracted and commented for both considered Hall structures.

Acknowledgments

The first author, Maria-Alexandra Paun, wishes to thank the Swiss National Science Foundation (SNSF) from Switzerland for the promotion and encouragement of the scientific research of young doctors, respectively by providing the funding for her postdoctoral fellowship at Cambridge University.

References

- [1] R.S. Popovic, *Hall Effect Devices: Magnetic Sensors and Characterization of Semiconductors*, Adam Hilger, Bristol, 1991.
- [2] A. Manzin, V. Nabaei, O. Kazakova, Modelling and optimization of submicron Hall sensors for the detection of superparamagnetic beads, *J. Appl. Phys.* 111 (Suppl. 7) (2012) 1–3 (07E513).
- [3] C.S. Roumenin, S.V. Lozanova, Linear displacement sensor using a new CMOS double-Hall sensor, *Sens. Actuators A* 138 (Issue 1) (2007) 37–43.
- [4] D. Manic, P.M. Igc, P.A. Mawby, Y. Haddab, R.S. Popovic, Mechanical stress related instabilities in silicon under metal coverage, *IEEE Trans. Electron. Devices* 47 (Suppl. 12) (2000) S2429–S2437.
- [5] A. Kerlain, V. Mosser, Dynamic low-frequency noise cancellation in quantum well Hall sensors (QWHS), *Sens. Actuators A* 142 (2008) 528–532.
- [6] R. Steiner, A. Haberli, F.-P. Steiner, C.h. Maier, H. Baltes, Offset reduction in Hall devices by continuous spinning current, *Sens. Actuators A* 66 (1998) 167–172.
- [7] C. Müller-Schwanneke, F. Jost, K. Marx, S. Lindenkreuz, K. von Klitzing, Offset reduction in silicon Hall sensors, *Sens. Actuators A* 81 (2000) 18–22.
- [8] S. Bellekom, P.M. Sarro, Offset reduction of Hall plates in three different crystal planes, *Sens. Actuators A* 66 (1998) 23–28.
- [9] J.B. Kammerer, L. Hebrard, V. Frick, P. Poure, F. Braun, Horizontal Hall effect sensor with high maximum absolute sensitivity, *IEEE Sensors* 3 (Suppl. 6) (2003) S700–S707.
- [10] M. Madec, J.-B. Kammerer, L. Hebrard, An improved compact model of cross-shaped CMOS-integrated Hall-effect sensors, in: *Proceedings of the NEWCAS Conference*, 2010, pp. 397–400.
- [11] Y. Hu, W.-R. Yang, CMOS Hall sensor using dynamic quadrature offset cancellation, in: *Proceedings of the ICSIT Conference*, 2006.
- [12] M. Pastre, M. Kayal, Automatic calibration of Hall sensor microsystems, *Microelectron. J.* 37 (2006) 1569–1575.
- [13] M.A. Paun, J.M. Sallese, M. Kayal, Comparative study on the performance of five different Hall effect devices, *Sensors* 13 (S 2) (2013) S2093–S2112.
- [14] M.A. Paun, J.M. Sallese, M. Kayal, Hall effect sensors design, integration and behaviour analysis, *J. Sens. Actuator Netw.* 2 (Issue 1) (2013) 85–97.
- [15] M.A. Paun, J.M. Sallese, M. Kayal, Geometrical parameters influence on the Hall effect sensors offset and drift, in: *Proceedings of the 7th Conference on Ph.D. Research in Microelectronics and Electronics (PRIME)*, 2011, pp. 145–148.
- [16] M.A. Paun, J.M. Sallese, M. Kayal, A specific parameters analysis of CMOS Hall effect sensors with various geometries, in: *Proceedings of the 19th International Conference on Mixed Design of Integrated Circuits and Systems (MIXDES)*, 2012, pp. 335–339.
- [17] M.A. Paun, J.M. Sallese, M. Kayal, Hall effect sensors performance investigation using three-dimensional simulations, in: *Proceedings of the 18th International Conference on Mixed Design of Integrated Circuits and Systems (MIXDES)*, 2011, pp. 450–455.
- [18] R.S. Popovic, *Hall Effect Sensors*, second edition, Institute of Publishing Bristol and Philadelphia, 2004.
- [19] W. Versnel, Analysis of symmetrical Hall plates with finite contacts, *J. Appl. Phys.* 52 (Suppl. 7) (1981) S4659–S4666.
- [20] M.A. Paun, J.M. Sallese, M. Kayal, Geometry influence on the Hall effect devices performance, *U.P.B. Sci. Bull. Ser. A* 72 (Suppl. 4) (2010) 257–271.
- [21] H. Blanchard, C.D. Iseli, R.S. Popovic, Compensation of the temperature-dependent offset drift of a Hall sensor, *Sens. Actuators A-Phys.* 60 (Suppl. 1–3) (1997) S10–S13.
- [22] H. Blanchard, R.S. Popovic, On chip compensation of the temperature dependent offset drift of Hall sensors, *Transducers '99*, in: *Proceedings of the 10th International Conference on Solid-State Sensors and Actuators*, Sendai, Japan, June 1999, pp. 598–601.

- [23] H. Blanchard, F. De Montmollin, J. Hubin, et al., Highly sensitive Hall sensor in CMOS technology, *Sens. Actuators A-Phys.* 82 (Suppl. 1–3) (2000) 144–148.
- [24] H. Blanchard, *Hall Sensors With Integrated Magnetic Flux Concentrators*, (PhD thesis), EPFL, Lausanne, Switzerland, 1999.
- [25] D. Manic, *Drift in Silicon Integrated Sensors and Circuits due to their Thermo-Mechanical Stresses*, (PhD thesis), EPFL, Lausanne, Switzerland, 2000.
- [26] D. Manic, P.M. Igit, Y. Haddab, R.S. Popovic, Mechanical stress related instabilities in silicon under metal coverage, *IEEE Trans. Electron Devices* 47 (Suppl. 12) (2000) 2429–2437.
- [27] G. Boero, M. Demierre, P.A. Besse, R.S. Popovic, Micro-Hall devices: performance, technologies and applications, *Sens. Actuators A* 106 (2003) 314–320.
- [28] A. Udo, M. Motz, M. Holliber, Drift of magnetic sensitivity of smart Hall sensors due to moisture absorbed by the IC-package, *Proc. IEEE Sens.* (2004) 455–458.
- [29] Synopsys TCAD software tools online documentation, access at the address: (<http://www.synopsys.com/Tools/TCAD>).
- [30] E. Ramsden, *Hall-Effect Sensors—Theory and Applications*, Second Edition, Elsevier, Burlington, USA, 2006.
- [31] S.M., Sze, K.K., Ng, “*Physics of Semiconductor Devices*”, Third Edition, John Wiley and Sons, 2007.
- [32] E., Jovanovic, T., Pesic, D., Pantic, 3D Simulation of Cross-shaped Hall Sensor and Its Equivalent Circuit Model, in: *Proceedings of the 24th International Conference on Microelectronics (MIEL)*, Vol. 1, 16–19 May, 2004, pp. 235–238.
- [33] M.A. Paun, *Hall Cells Offset Analysis and Modeling Approaches*, (PhD thesis), EPFL, Switzerland, 2013.
- [34] M.A. Paun, J.M. Sallèse, M. Kayal, Temperature considerations on Hall Effect sensors current-related sensitivity behaviour, *Analog Integr. Circuits Signal Process.* 77 (Suppl. 3) (2013) S355–S364.
- [35] M.A., Paun, J.M., Sallèse, M., Kayal, “*A circuit model for CMOS Hall Cells Performance Evaluation Including Temperature Effects*”, *Advances in Condensed Matter Physics*, Vol. 2013, Article ID 968647, 10 pages, 2013.